Research Article | Vol. 33, No. 13 / 30 Jun 2025 / Optics Express 26930

Optics EXPRESS

Comparison of near-field light intensities: plasmon nanofocusing versus localized plasmon resonance

TONGYAO LI,[1] ANDREA SCHIRATO,[2,3] TAKU SUWABE,[1] REMO PROIETTI ZACCARIA,[4] PRABHAT VERMA,[1] AND TAKAYUKI UMAKOSHI[1,5,*]

[1] Department of Applied Physics, Osaka University, 2-1 Yamadaoka, Suita, Osaka 565-0871, Japan
[2] Department of Physics, Politecnico di Milano, Piazza Leonardo da Vinci 32, Milano 20133, Italy
[3] Department of Physics and Astronomy, Rice University, Houston, Texas 77005, USA
[4] Istituto Italiano di Tecnologia, Via Morego 30, Genova 16163, Italy
[5] Institute for Advanced Co-Creation Studies, Osaka University, 2-1 Yamadaoka, Suita, Osaka 565-0871, Japan
[*] umakoshi@ap.eng.osaka-u.ac.jp

Abstract: The localized surface plasmon resonance of metallic nanostructures produces strongly localized and enhanced near-field light, significantly contributing to nanophotonics research and applications. Plasmon nanofocusing represents another method for generating near-field light through the propagation and condensation of plasmons on tapered plasmonic structures. In both methods, the intensity of near-field light is a critical aspect for many applications. In this study, we numerically inspect and compare the intensities of near-field light generated by either localized plasmon resonance or plasmon nanofocusing. To account for the light-induced changes in the optical properties of plasmonic structures, which in turn influence the near-field light intensity, we couple electromagnetic and thermal calculations to consider in a fully self-consistent manner the effects of the incident light and the light-induced temperature rise within the metal. A gold nanorod and a cone were adopted for exciting the localized plasmon resonance and plasmon nanofocusing, respectively. We find that plasmon nanofocusing generates approximately 1.5 times as strong near-field light as localized plasmon resonance. Our research provides a necessary foundation for generating near-field light, which is crucial for advancing the applications of near-field optics.

1. Introduction

Strongly localized and enhanced near-field light produced by plasmonic nanostructures has been widely applied in various fields from material science to biology, having realized a number of optical applications in the past few decades, such as enhanced optical spectroscopy, super-resolution microscopy, light harvesting, plasmonic lasers [1–8]. Near-field light is usually achieved by exciting the localized surface plasmon resonance (LSPR) of metallic nanostructures that work as optical antennas, with gold nanoparticles and nanorods being among the most typically employed systems [9,10]. In recent years, plasmon nanofocusing has caught considerable attention as another method for generating near-field light. In the process of plasmon nanofocusing, surface plasmon polaritons propagate along a metallic tapered structure, such as a gold conical structure, toward the apex while compressing their energy, and eventually create strong near-field light at the nanometrically sharp apex [11–14]. A grating structure fabricated on the shaft of a tapered structure is often used as a coupler to excite plasmons. Because the grating structure is located far from the apex, one of the advantages of nanofocusing is that it is background-free from incident light, contrary to the LSPR approach, where the direct incident light illumination

#563279 https://doi.org/10.1364/OE.563279
Journal © 2025 Received 25 Mar 2025; revised 20 Apr 2025; accepted 11 May 2025; published 16 Jun 2025

Optics EXPRESS

of plasmonic nanostructures spatially overlaps with near-field light [15–18]. The broadband characteristic of plasmon nanofocusing has also recently been recognized as another unique property. Plasmon nanofocusing can be achieved over a wide frequency range, because it is based on the propagation of plasmons, unlike plasmon resonances occurring within a specific spectral range [19–22].

Considering the two methods of LSPR and plasmon nanofocusing, one of the fundamental but pivotal questions is which method generates more intense near-field light, as the near-field light intensity is a basic and important optical property for many applications. With respect to LSPR, the strength of near-field light has often been described as the enhancement factor, which is calculated as the ratio of the near-field light intensity to the incident light intensity. For plasmon nanofocusing, the amount of incident light energy converted to near-field light, that is, the conversion efficiency, has usually been investigated. Although the enhancement factor and efficiency are important for evaluating the near-field light intensity, they are normalized by the incident light intensity. As such, they do not provide direct information on the absolute value of the near-field light intensity for both methods, which in fact can also be critical from an application standpoint. In particular, upon increasing the incident light intensity, which in turn increases the near-field light intensity, plasmonic structures can be melted and irreversibly destroyed due to the heat generated by ohmic losses [23–27]. This suggests that the maximum threshold incident light intensity can be defined as the one causing a temperature increase right below the melting point of plasmonic structures. In these terms, the photogeneration of heat contributing to the temperature rise is a key factor to gauge the maximum allowed incident light intensity and the corresponding maximum near-field light intensity for both LSPR and plasmon nanofocusing.

In this study, we numerically investigated which between LSPR and plasmon nanofocusing generates more intense near-field light, by including the effects of light-induced heat generation and temperature rise in plasmonic structures. We selected a gold nanorod and a gold cone as the plasmonic systems typically used for the excitation of LSPR and plasmon nanofocusing, respectively. We examined the temperature and near-field light intensity by varying the incident light intensity. The maximum incident light intensities and the resulting maximum near-field light intensities were evaluated, and were found to be different between LSPR and plasmon nanofocusing, owing to the difference in the geometrical configurations between the gold nanorod and cone. We found that plasmon nanofocusing allows for achieving a higher near-field light intensity than LSPR when optimal input powers were exerted on each structure. As for plasmon nanofocusing, we also observed a saturation followed by an inverse change in the near-field light intensity with respect to the incident light intensity, which our model explained by coupling electromagnetic and thermal problems consistently. Finally, since the melting temperature of gold (1337 K) is relatively high for most applications, we also considered moderate illumination conditions and temperature increases up to 40°C (313.15 K) and 100°C (373.15 K), which are relevant for practical situations [28].

2. Calculation model

We used the finite element method-based commercial software COMSOL Multiphysics to calculate the steady-state electric field intensity and temperature field of the plasmonic structures under scrutiny. The schematics of our numerical models are shown in Fig. 1. We chose 785 nm as the incident light wavelength, which is typical in various optical measurements and applications. The incident light has a Gaussian space profile, with a beam waist of 550 nm. Both nanostructures are embedded in air. For the gold nanorod, we set the rod diameter and length to 20 and 105 nm, respectively, to tune the longitudinal LSPR wavelength to 785 nm (Fig. S1). As for the gold cone, the cone apex size is 20 nm, which is the same as the gold nanorod diameter, so that the plasmonic confinement of near-field light is comparable with that of the nanorod. The cone

Optics EXPRESS

length was set to 7 µm. We designed a grating structure 3.75 µm away from the apex, which is far enough to separate the incident light from the near-field light. It is composed of three grooves, whose period and depth are 680 and 100 nm, respectively, and it is optimized for the best plasmon coupling efficiency at a wavelength of 785 nm, as shown in Fig. S2. The entire gold nanorod was exposed to illumination, whereas the grating structure was irradiated by the incident light for the gold cone, as illustrated in Figs. 1(a) and 1(b). Therefore, the grating can receive a greater number of photons owing to its large structure compared with the small nanorod in the same illumination condition, which is another characteristic of plasmon nanofocusing.

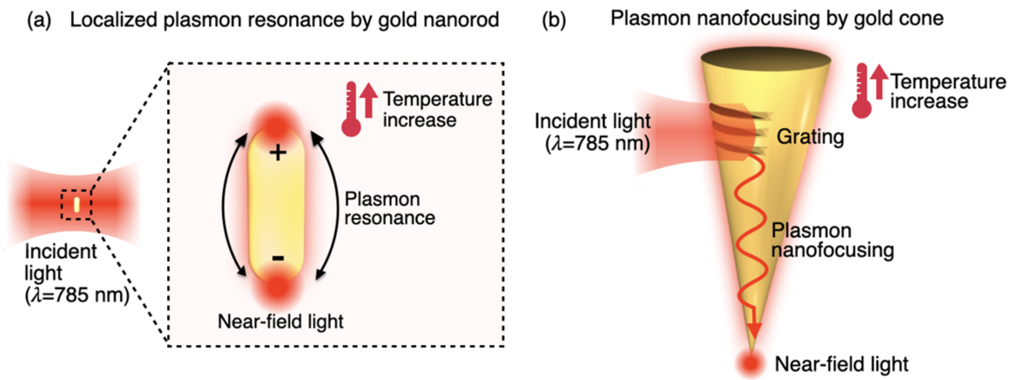

Fig. 1. Schematics of calculation models of (a) localized plasmon resonance and (b) plasmon nanofocusing

For the gold nanorod and the cone, the electric field intensity and temperature were calculated by solving Maxwell's equations coupled to the heat transfer. The initial temperature was set to room temperature (293.15 K/20 °C). When the incident light irradiates the structure, not only near-field light but also Joule heating is generated, following photon absorption and subsequent electromagnetic dissipation, which leads to a temperature increase in these metallic structures [29,30]. In turn, the permittivity of gold is modified by such an increase of the metal temperature. Specifically, we accounted for this effect by considering a temperature-dependent damping factor in an analytical Drude-Lorentz-like permittivity, which is suited for gold in this wavelength range [31–33]. The change in the permittivity of gold alters the electromagnetic response of the plasmonic system, including the near-field light intensity and electric field inside the gold structures, causing a change in the amount of Joule heating. Therefore, by coupling the optical and photothermal responses of the considered nanostructures, our numerical model treats this interdependence fully consistently until convergence to the steady state. The calculation details are thoroughly described in Supplement 1 Note S1.

3. Results and discussion

We first investigated the effects of exciting the LSPR of the nanorod. As shown in Fig. 2(a), when the gold nanorod is irradiated, near-field light appears at both ends of the nanorod, which is the typical electric field distribution of the longitudinal plasmonic mode of nanorods. Here, the incident light intensity was set to 1.33×10^7 W/m^2, by referring to the maximum intensity at the center of the Gaussian distribution of the incident light, which corresponds to a total power of 12.6 µW. This incident intensity produced a near-field light intensity of 2.75×10^9 W/m^2, indicating an approximately 207 times intensity enhancement. In particular, the near-field light intensity was monitored 3 nm away from the end of the gold nanorod. As expected, when the incident light intensity increased, the near-field light intensity also increased, as shown in Figs. 2(b) and

Optics EXPRESS

2(c). Specifically, we obtained near-field light intensities of 14.92×10^9 and 47.77×10^9 W/m^2 when the incident light intensities increased to 8.31×10^7 and 47.79×10^7 W/m^2, indicating intensity enhancements of ~ 180 and ~ 101 times, respectively. Interestingly, the enhancement of the electric field intensity decreased with increasing incident light intensity. We ascribe this saturation effect to the larger damping factor at higher temperatures, as described in detail in the following. For comparison, results obtained assuming a constant damping factor are also presented (see Fig. S3). The temperature distributions were then calculated for the same incident light intensities, as shown in Figs. 2(d)–2(f). The temperature was uniform over the gold nanorod because of the high thermal diffusion of the metal, in stark contrast with the inhomogeneous electric field distributions. As expected, the temperature also increased as the incident light intensity increased. When the incident light intensity was 1.33×10^7 W/m^2, the temperature, evaluated as the surface average over the entire gold nanorod, increased from 293.15 K to 318 K. It increased to 418 and 721 K with incident light intensities of 8.31×10^7 and 47.79×10^7 W/m^2, respectively.

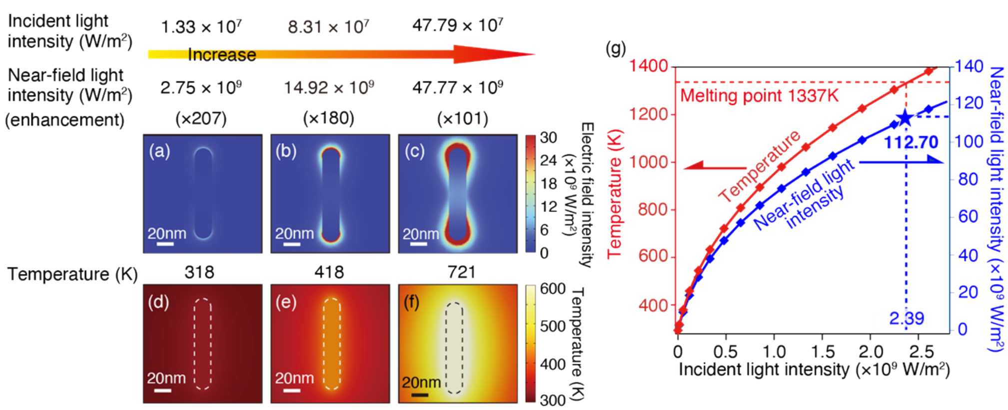

Fig. 2. Electric field distributions at incident light intensities of (a) 1.33×10^7, (b) 8.31×10^7, and (c) 47.79×10^7 W/m^2. Temperature distributions at the same incident light intensities of (d) 1.33×10^7 (318 K), (e) 8.31×10^7 (418 K), and (f) 47.79×10^7 (721 K). (g) Dependence of near-field light intensity and temperature of the gold nanorod on the incident light intensity.

To further inspect the dependence of the near-field light intensity and light-induced temperature increase upon increasing the illumination intensity, as shown in Fig. 2(g), we varied the incident light intensity up to 2.80×10^9 W/m^2, to reach a temperature close to the melting point of gold (1337 K, as indicated by the red dashed line). Both the near-field light intensity and temperature increased as the incident light intensity increased, yet following a sub-linear behavior. The nonlinear change in the near-field light intensity is explained as the result of the change in the damping factor of gold. We found that the maximum near-field light intensity, that is, slightly below the melting point, was 112.70×10^9 W/m^2, corresponding to an incident light intensity of 2.39×10^9 W/m^2.

Please note that the melting point of 1337 K is for bulk gold [34]. However, the melting point can be reduced for nano-sized materials due to the effects of size. In fact, the reduction in the melting point was estimated to be only a few tens of degrees for a gold nanosphere with a diameter of 10 nm, according to previous studies [34–36]. Compared to the 10-nm-large gold nanospheres, the size effect should be much smaller for the 105-nm-long gold nanorod. In addition, it is not straightforward to accurately evaluate the size effect on the melting point decrement of the gold nanorod. Therefore, we ignored the size effect and used the melting point of bulk gold in this

Optics EXPRESS

study. If the size effect is considered, the maximum incident light intensity and the resulting near-field light intensity should be slightly lower.

For plasmon nanofocusing on the gold cone, we also investigated the electric field intensity and temperature in a manner similar to that detailed above for the gold nanorod. Figure 3(a) shows the electric field distribution map around the gold cone structure under the incident light illumination of the grating coupler with an intensity of 107.73×10^7 W/m^2. Surface plasmons were excited at the grating and propagated along the surface of the gold cone structure, generating highly confined near-field light at the apex. The enlarged map around the apex is shown in Fig. 3(d), which clearly confirms plasmon nanofocusing inducing the near-field light at the apex. The near-field light intensity obtained at 3 nm away from the tip apex was 94.09×10^9 W/m^2, indicating an intensity enhancement of ~ 87 times. The temperature distribution under the same condition is shown in Fig. 3(b). Similar to the gold nanorod, the temperature uniformly increased to 420 K over the entire gold cone. The enlarged temperature map around the apex is also shown in Fig. 3(g). We then reduced the incident intensity to 11.97×10^7 W/m^2 (Fig. 3(c)) and increased it to 430.92×10^7 W/m^2 (Fig. 3(e)). With a smaller incident light intensity of 11.97×10^7 W/m^2, we obtained a near-field light intensity of 13.08×10^9 W/m^2. The near-field light intensity was 178.39×10^9 W/m^2 in the case of a larger incident light intensity of 430.92×10^7 W/m^2. Therefore, similar to the case of LSPR, the near-field light intensity increased with the incident light intensity in the plasmon nanofocusing. Accordingly, the temperature was also increased from 307 to 805 K by increasing the incident light intensity from 11.97×10^7 to 430.92×10^7 W/m^2, as shown in Figs. 3(f)–(h).

Furthermore, we extensively investigated the dependences of near-field light intensity and temperature increase on the incident light intensity, as shown in Fig. 3(i). We changed the incident light intensity up to 10.00×10^9 W/m^2. Interestingly, the near-field light intensity first increases with increasing incident light intensity, and subsequently decreases even though the incident light intensity increases. In contrast, the temperature monotonically increases with the incident light intensity across the entire range we spanned. The linear increase in temperature, which differs from the nonlinear behavior of the gold nanorod, can be due to the size of the gold cone. The gold cone is much larger than the gold nanorod, which can lead to a larger heat capacity and a linear temperature increase. The counterintuitive highly nonlinear inverse trend in the near-field light intensity is explained by the fact that, as mentioned previously, a higher temperature produces a larger damping factor of gold, which negatively influences the near-field light intensity to be reduced. Although increasing the incident light intensity simply increases the near-field light intensity, the higher temperature caused by the larger incident light intensity causes a reduction in the near-field light intensity. Therefore, depending on the balance between these two effects, the near-field light intensity can be decreased even upon increasing the incident light intensity. In particular, because plasmon nanofocusing involves the propagation of plasmons for a certain distance, the damping factor can dominate the process to a larger extent than LSPR, which does not involve propagation. We therefore evaluated the decrement of near-field light intensity due to larger damping factors at high temperatures for plasmon nanofocusing. We found indeed that this effect impacted more dominantly than the increment of near-field light intensity for increasing incident light intensities, leading thus to the reduction of near-field light intensity (as discussed in detail in Supporting Information Note S5).

In plasmon nanofocusing, we found that the maximum near-field light intensity of 178.45×10^9 W/m^2 was achieved for an incident light intensity of 4.55×10^9 W/m^2, where the temperature was 834 K. The near-field light intensity monotonically decreased for incident light intensities greater than this value. When the temperature approached the melting point, the near-field light intensity was 138.53×10^9 W/m^2, where the incident light intensity was 8.99×10^9 W/m^2. Therefore, we concluded that the maximum near-field light intensity obtained by plasmon nanofocusing on the gold cone was 178.45×10^9 W/m^2. As the maximum near-field light intensity was 112.70×10^9

Optics EXPRESS

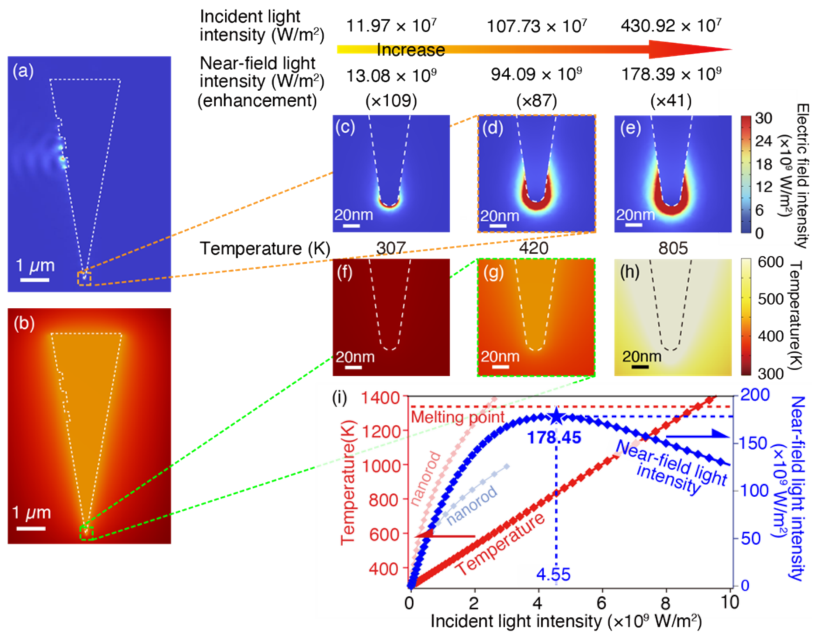

Fig. 3. (a) Electric field distribution and (b) temperature distribution of the gold cone at an incident light intensity of 107.73×10^7 W/m^2. Electric field distribution maps enlarged near the apex at incident light intensities of (c) 11.97×10^7, (d) 107.73×10^7, and (e) 430.92×10^7 W/m^2. Temperature distribution maps enlarged near the apex at incident light intensities of (f) 11.97×10^7 (307 K), (g) 107.73×10^7 (420 K), and (h) 430.92×10^7 W/m^2 (805 K). (i) Dependence of the near-field light intensity and temperature of the gold cone on the incident light intensity. For comparison, the near-field light intensity and temperature obtained for the gold nanorod are also shown as light blue and red curves, respectively, which were obtained from Fig. 2(g).

W/m^2 for LSPR, plasmon nanofocusing induces near-field light approximately 1.5 times stronger than that for LSPR.

So far, we have considered a temperature close to the melting point; however, this is not practical as the temperature of the melting point is too high for most applications and rather sets an upper boundary of operation. Therefore, we investigated the illumination conditions required to reach moderate maximum temperatures, such as 40°C (Fig. 4(a)) and 100°C (Fig. 4(b)). Here, we increased the incident light intensity up to 80.00×10^7 W/m^2. Temperatures of 40°C (313.15 K) and 100°C (373.15 K) are indicated by the green and orange dashed lines, respectively. Both the near-field light intensities and temperatures increase as the incident light intensity increases for both the gold nanorod and cone. It is evident that the temperature of the gold nanorod rises quickly with the incident light intensity due to its smaller size compared to the gold cone. Therefore, the temperature easily reached the limit (40 or 100°C) with low incident light intensities. At a temperature of 40°C, the near-field light intensity generated by LSPR was only 2.41×10^9 W/m^2 (corresponding to an incident light intensity of 1.08×10^7 W/m^2), whereas the near-field light intensity generated by plasmon nanofocusing was 18.35×10^9 W/m^2 (incident light intensity: 16.99×10^7 W/m^2). We thus found that plasmon nanofocusing generated near-field light ~7.6 times stronger than that generated by LSPR to reach the same temperature. Considering a temperature of 100°C, the near-field light intensity was 9.63×10^9 W/m^2 for LSPR (incident light intensity of 4.90×10^7 W/m^2). In contrast, the near-field light intensity generated by plasmon nanofocusing was 64.87×10^9 W/m^2 (incident light intensity: 67.77×10^7

Optics EXPRESS

W/m^2), which was ~6.7 times stronger than that of LSPR. These results indicate that plasmon nanofocusing is more advantageous as it generates significantly stronger near-field light compared to LSPR when used in a practical situation at a moderate temperature.

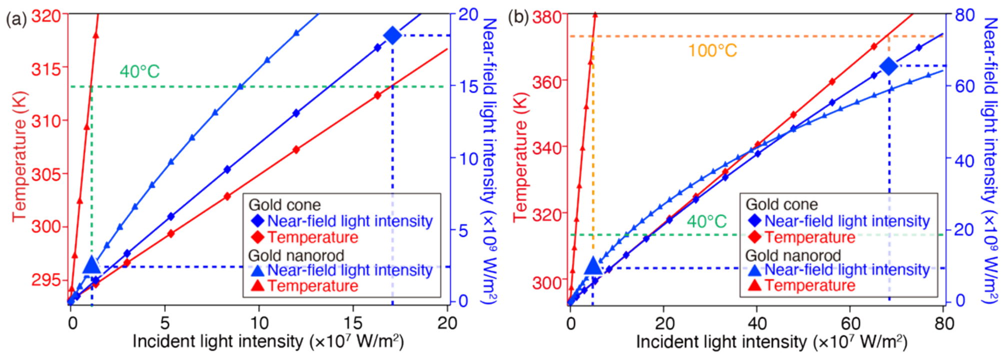

Fig. 4. Dependences of the near-field light intensity and temperature on the incident light intensity at a lower intensity range for the gold nanorod and cone. Lower temperature limitations of (a) 40°C and (b) 100°C were considered.

4. Conclusion

In conclusion, we investigated which between LSPR or plasmon nanofocusing generates stronger near-field light. The maximum near-field light intensity was determined by considering the light-induced heat generation and temperature increase in the gold structures. It was 112.70×10^9 W/m^2 for LSPR of the gold nanorod, whereas it was 178.45×10^9 W/m^2 for plasmon nanofocusing of the gold cone, when the incident light intensities were 2.39×10^9 and 4.55×10^9 W/m^2, respectively. Therefore, plasmon nanofocusing generates approximately 1.5 times as strong near-field light as that generated by LSPR. Moreover, the near-field intensity could be enhanced more by further optimizing the gold cone geometrical parameters, including the cone angle and the grating structure. We used a cone angle of 28 degrees. Although a smaller angle is better for adiabatic nanofocusing, it can reduce the size of the grating and the amount of excited plasmons. Furthermore, while the distance between the grating and the tip in our calculations was limited to 3.75 µm due to the machine power, a longer distance is preferable to reduce the influence of incident light while increasing the plasmon propagation loss.

The input powers are in the range of several milliwatts within a micrometer-order focal spot, which is not far from our expectation of causing the destruction of gold nanostructures [37]. We thus believe that our simulation results are within a reasonable range compared with actual experiments. The experimental validation of our calculations could be achieved, for instance, by Raman spectroscopy, which measures a local temperature through the intensity ratio of Stokes and anti-Stokes Raman signals. Note that some differences are anticipated between our simulations and actual experiments. For example, the gold structures suspended in air were considered in our simulations, whereas gold structures are usually placed on a substrate in actual experiments, which can have a relevant role in dissipating heat. The thermal conductivities of typical substrates (e.g., glass or silicon) are much higher than that of air. Therefore, they facilitate thermal diffusion, which are expected to increase the maximum threshold incident light intensity and the resulting near-field light intensity.

Considering lower temperature regions, plasmon nanofocusing was more effective, as several times stronger near-field light was obtained compared with LSPR. These results provide crucial insights for actual applications when integrated into plasmonic platforms or devices for stronger

Optics EXPRESS

near-field light while maintaining a sufficiently low temperature. In addition, our investigation will be important for the study of fragile biological samples, which are prone to be degraded at high temperatures. In this study, we only considered the specific condition with the gold nanorod and cone with an incident wavelength of 785 nm. The results can differ between different materials and shapes of the plasmonic structures. For example, silver is another representative plasmonic material with a slightly higher thermal conductivity and lower melting point than gold. TiN_2 is an interesting plasmonic material with a high melting point (3203 K) and a very low thermal conductivity (29 W/(m·K)) [38]. Moreover, it is worth investigating not only the typical dipole mode considered in this study, but also various types of resonance modes, such as the magnetic dipole, toroidal dipole, and anapole modes [39–41]. More extensive studies as future works under various conditions, exploiting the comparative approach proposed here, are crucial for elucidating the near-field light intensity for both LSPR and plasmon nanofocusing. This fundamental study provides important and practical insights relevant to various applications based on nanophotonics and plasmonics.

Funding. Japan Society for the Promotion of Science (24K01385, 23H04590, 24H01717, 24K21718); Fusion Oriented REsearch for disruptive Science and Technology (JPMJFR233Z); Takahashi Industrial and Economic Research Foundation; HORIZON EUROPE Marie Sklodowska-Curie Actions (101153856).

Acknowledgment. We acknowledge Mr. Zhen Zong (Osaka University) for his support to our calculations.

Disclosures. The authors declare no conflicts of interest.

Data availability. Data underlying the results presented in this paper are not publicly available at this time but may be obtained from the authors upon reasonable request.

Supplemental document. See Supplement 1 for supporting content.

References

1. S. Kawata, Y. Inouye, and P. Verma, "Plasmonics for near-field nano-imaging and superlensing," Nat. Photonics **3**(7), 388–394 (2009).
2. P. Verma, "Tip-Enhanced Raman Spectroscopy: Technique and Recent Advances," Chem. Rev. **117**(9), 6447–6466 (2017).
3. T. Umakoshi, K. Kawashima, T. Moriyama, *et al.*, "Tip-enhanced Raman spectroscopy with amplitude-controlled tapping-mode AFM," Sci. Rep. **12**(1), 12776 (2022).
4. Y. Tian and T. Tatsuma, "Mechanisms and Applications of Plasmon-Induced Charge Separation at TiO2 Films Loaded with Gold Nanoparticles," J. Am. Chem. Soc. **127**(20), 7632–7637 (2005).
5. R. F. Oulton, V. J. Sorger, T. Zentgraf, *et al.*, "Plasmon lasers at deep subwavelength scale," Nature **461**(7264), 629–632 (2009).
6. Y. Lu, J. Kim, H. Y. Chen, *et al.*, "Plasmonic Nanolaser Using Epitaxially Grown Silver Film," Science **337**(6093), 450–453 (2012).
7. H. M. Chen, C. K. Chen, C. J. Chen, *et al.*, "Plasmon Inducing Effects for Enhanced Photoelectrochemical Water Splitting: X-ray Absorption Approach to Electronic Structures," ACS Nano **6**(8), 7362–7372 (2012).
8. M. L. Tseng, C. M. Chang, B. H. Cheng, *et al.*, "Multi-level surface enhanced Raman scattering using AgOx thin film," Opt. Express **21**(21), 24460–24467 (2013).
9. W. L. Barnes, A. Dereux, and T. W. Ebbesen, "Surface plasmon subwavelength optics," Nature **424**(6950), 824–830 (2003).
10. L. Vigderman, B. P. Khanal, E. R. Zubarev, *et al.*, "Functional Gold Nanorods: Synthesis, Self-Assembly, and Sensing Applications," Adv. Mater. **24**(36), 4811–4841 (2012).
11. A. J. Babadjanyan, N. L. Margaryan, Kh. V. Nerkararyan, *et al.*, "Superfocusing of surface polaritons in the conical structure," J. Appl. Phys. **87**(8), 3785–3788 (2000).
12. M. I. Stockman, "Nanofocusing of Optical Energy in Tapered Plasmonic Waveguides," Phys. Rev. Lett. **93**(13), 137404 (2004).
13. H. Choo, M. Kim, M. Staffaroni, *et al.*, "Nanofocusing in a metal–insulator–metal gap plasmon waveguide with a three-dimensional linear taper," Nat. Photonics **6**(12), 838–844 (2012).
14. R. P. Zaccaria, A. Alabastri, F. D. Angelis, *et al.*, "Fully analytical description of adiabatic compression in dissipative polaritonic structures," Phys. Rev. B **86**(3), 035410 (2012).
15. C. Ropers, C. C. Neacsu, T. Elsaesser, *et al.*, "Grating-coupling of surface plasmons onto metallic tips: a nanoconfined light source," Nano Lett. **7**(9), 2784–2788 (2007).
16. T. Umakoshi, Y. Saito, and P. Verma, "Highly efficient plasmonic tip design for plasmon nanofocusing in near-field optical microscopy," Nanoscale **8**(10), 5634–5640 (2016).

Optics EXPRESS

17. C. C. Neacsu, S. Berweger, R. L. Olmon, *et al.*, "Near-field localization in plasmonic superfocusing: a nanoemitter on a tip," Nano Lett. **10**(2), 592–596 (2010).
18. S. Berweger, J. M. Atkin, R. L. Olmon, *et al.*, "Light on the Tip of a Needle: Plasmonic Nanofocusing for Spectroscopy on the Nanoscale," J. Phys. Chem. Lett. **3**(7), 945–952 (2012).
19. T. Umakoshi, M. Tanaka, Y. Saito, *et al.*, "White nanolight source for optical nanoimaging," Sci. Adv. **6**(23), eaba4179 (2020).
20. K. Taguchi, T. Umakoshi, S. Inoue, *et al.*, "Broadband plasmon nanofocusing: Comprehensive study of broadband nanoscale light source," J. Phys. Chem. C **125**(11), 6378–6386 (2021).
21. M. Esmann, S. F. Becker, J. Witt, *et al.*, "Vectorial near-field coupling," Nat. Nanotechnol. **14**(7), 698–704 (2019).
22. V. Kravtsov, R. Ulbricht, J. M. Atkin, *et al.*, "Plasmonic nanofocused four-wave mixing for femtosecond near-field imaging," Nat. Nanotechnol. **11**(5), 459–464 (2016).
23. X. Cui, Q. Ruan, X. Zhuo, *et al.*, "Photothermal Nanomaterials: A Powerful Light-to-Heat Converter," Chem. Rev. **123**(11), 6891–6952 (2023).
24. L. Jauffred, A. Samadi, H. Klingberg, *et al.*, "Plasmonic Heating of Nanostructures," Chem. Rev. **119**(13), 8087–8130 (2019).
25. B. Yang, C. Li, Z. Wang, *et al.*, "Thermoplasmonics in Solar Energy Conversion: Materials, Nanostructured Designs, and Applications," Adv. Mater. **34**(26), 2107351 (2022).
26. A. Lalisse, G. Tessier, J. Plain, *et al.*, "Quantifying the Efficiency of Plasmonic Materials for Near-Field Enhancement and Photothermal Conversion," J. Phys. Chem. C **119**(45), 25518–25528 (2015).
27. K. Nishita, G. Deka, N. I. Smith, *et al.*, "Nonlinear Scattering of Near-Infrared Light for Imaging Plasmonic Nanoparticles in Deep Tissue," ACS Photonics **7**(8), 2139–2146 (2020).
28. G. Baffou, F. Cichos, and R. Quidant, "Applications and challenges of thermoplasmonics," Nat. Mater. **19**(9), 946–958 (2020).
29. A. O. Govorov and H. H. Richardson, "Generating Heat With Metal Nanoparticles," Nano Today **2**(1), 30–38 (2007).
30. G. Baffou and R. Quidant, "Thermo-plasmonics: using metallic nanostructures as nano-sources of heat," Laser & Photonics Reviews **7**(2), 171–187 (2013).
31. A. D. Rakic, A. B. Djurišić, J. M. Elazar, *et al.*, "Optical properties of metallic films for vertical-cavity optoelectronic devices," Appl. Opt. **37**(22), 5271–5283 (1998).
32. P. B. Johnson and R. W. Christy, "Optical Constants of the Noble Metals," Phys. Rev. B **6**(12), 4370–4379 (1972).
33. A. Alabastri, S. Tuccio, A. Giugni, *et al.*, "Molding of Plasmonic Resonances in Metallic Nanostructures: Dependence of the Non-Linear Electric Permittivity on System Size and Temperature Only this one," Materials **6**(11), 4879–4910 (2013).
34. P. Buffat and J. P. Borel, "Size effect on the melting temperature of gold particles," Phys. Rev. A **13**(6), 2287–2298 (1976).
35. G. L. Allen, R. A. Bayles, W. W. Gile, *et al.*, "Small particle melting of pure metals," Thin Solid Films **144**(2), 297–308 (1986).
36. A. Safaei, M. A. Shandiz, S. Sanjabi, *et al.*, "Modelling the size effect on the melting temperature of nanoparticles, nanowires and nanofilms," J. Phys.: Condens. Matter **19**(21), 216216 (2007).
37. M. Honda, Y. Saito, N. I. Smith, *et al.*, "Nanoscale heating of laser irradiated single gold nanoparticles in liquid," Opt. Express **19**(13), 12375–12383 (2011).
38. M. Tamura, T. Iida, and K. Setoura, "Plasmonic nanoscale temperature shaping on a single titanium nitride nanostructure," Nanoscale **14**(35), 12589–12594 (2022).
39. A. Hassanfiroozi, Z. S. Huang, W. H. Cheng, *et al.*, "Vertically-Stacked Discrete Plasmonic Meta-Gratings for Broadband Space-Variant Metasurfaces," Adv. Opt. Mater. **11**(8), 2202717 (2023).
40. A. Hassanfiroozi, P. S. Huang, S. H. Huang, *et al.*, "A Toroidal-Fano-Resonant Metasurface with Optimal Cross-Polarization Efficiency and Switchable Nonlinearity in the Near-Infrared," Adv. Opt. Mater. **9**(21), 2101007 (2021).
41. P. C. Wu, C. Y. Liao, V. Savinov, *et al.*, "Optical Anapole Metamaterial," ACS Nano **12**(2), 1920–1927 (2018).